Macromolecules

Article

pubs.acs.org/Macromolecules

# Conformational Transitions of Poly(L-proline) in Copolypeptides with Poly(γ-benzyl-L-glutamate) Induced by Packing

R. Graf,*[,†] H. W. Spiess,[†] G. Floudas,[†,‡] H.-J. Butt,[†] M. Gkikas,[§] and H. Iatrou*[,§]

[‡]Department of Physics, University of Ioannina, P.O. Box 1186, GR-45110 Ioannina, Greece

[†]Max-Planck-Institut für Polymerforschung, D-55021 Mainz, Germany

[§]Department of Chemistry, University of Athens, Panepistimiopolis, Zografou, GR-15771 Athens, Greece

Supporting Information

**ABSTRACT:** The hierarchical self-assembly and dynamics of poly(γ-benzyl-L-glutamate)-*b*-poly(L-proline) (PBLG-*b*-PLP) polypeptides are investigated with X-rays and solid state NMR. Both blocks possess helices stabilized solely either by hydrogen bonds (PBLG) or by steric hindrance (PLP) and are further packed in two different hexagonal cells. We report a *trans*/*cis* conformational change of PLP upon confinement that mimics the isomerization of isolated proline residues in proteins. These *cis* PLP conformations reside primarily at the PLP/PBLG interface, alleviate the packing frustration, and permit PBLG and PLP helices to pack with their bulk properties.

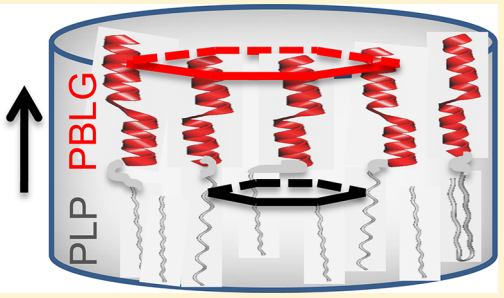


## I. INTRODUCTION

Proline residues are of exceptional significance in protein conformation and protein folding.[1,2] It has been suggested that isolated proline residues play an important role in the regulation of transmembrane proteins through the *cis*/*trans* isomerization—and the resulting redirection of the protein chains—that is proposed to assist ion translocation.[3,4] This situation is different in peptide bonds formed by other amino acids as they are generally planar and *trans*. Furthermore, the role of proline residues as α-helix "brakers" has been explored.[5] It was found that proline residues in the center of α-helices produce a sharp kink that gives rise to two halves of the helix at an angle of ∼26°. The proline residues responsible for the kinks have been conserved during the course of protein evolution suggesting an underlying structural and functional role. It is also documented that proline residues occur not only as isolated but are found at a much higher fractions than average in many proteins.[4] Proline-rich proteins from several sources have been identified and characterized including viruses, e.g. the nuclear protein in Epstein−Barr virus has a mimium of 29 proline residues in succession.

The reason behind these unique properties and functions is a property of the proline residue: Proline is the only one among the amino acids where the nitrogen bears no amide hydrogen, thus making hydrogen bonding impossible. Furthermore, the bulky pyrrolidine ring restricts the available conformations giving rise to unique forms. As a result the *cis* configuration of the imide group is much more probable as compared to other amino acids. The activation energy barrier for *cis*−*trans* isomerization is also lower than in other peptide bonds.[6] The above peculiarities give rise to two poly(L-proline) forms:[7,8] Form I has *cis* peptide bonds forming a compact right-handed helix with a $10_3$ symmetry, comprising 3.33 residues per turn and a residue repeat (i.e., axial translation per residue) of 1.9 Å. Form II has *trans* peptide bonds and forms either a left-handed helix with $3_1$ symmetry, 3 residues per turn, and a residue repeat of 3.12 Å, or a right-handed helix with $2_1$ symmetry, 2 residues per turn and a residue repeat of 2.80 Å. In any case, form II is highly extended. The above should be compared with the α-helix of poly(γ-benzyl-L-glutamate) (PBLG) with $18_5$ symmetry, 3.6 residues per turn and a residue repeat of only 1.50 Å.[9−12] Furthermore, poly(L-proline) I is stable in poor solvents where the intrachain interactions are preferred over the polymer−solvent interactions. It transforms to form II in the presence of water, organic acids, and some organic solvents. The conformational isomerization from form I to form II can be studied by measuring the rate of mutarotation or the rate of the circular dichroism spectrum.

Recently the synthesis of well-defined homopolymers of L-proline has been reported by using the Boc-protected, rather than the free amino acid.[13] In addition, the synthesis of well-defined block copolymers based on poly(L-proline) (PLP) and PBLG was reported.[13] The latter is of particular interest as it refers to copolypeptides where the two blocks possess helices stabilized solely either by hydrogen bonds (PBLG) or by steric hindrance (PLP) (see Scheme 1). Herein we select two such copolypeptides and investigate the effect of nanophase confinement on the stability and coherence of the secondary structures by structural (wide-angle X-ray scattering, WAXS, solid state NMR) and dynamic (NMR) means. We find a *trans*/*cis* change of the PLP conformation upon confinement that mimics the isomerization of isolated proline residues in

**Received:** September 11, 2012
**Revised:** November 13, 2012
**Published:** November 16, 2012

   dx.doi.org/10.1021/ma301906m | *Macromolecules* 2012, 45, 9326−9332

**Scheme 1. (Top) Schematic of the PBLG-*b*-PLP copolymer structure. (Bottom) Schematic of a $PBLG_{14}$-*b*-$PLP_{12}$ in the "ideal" fully extended conformation (red, O; blue, N; gray, C, white, H). Notice that the phenyl rings of PBLG are not included on the lower schematic**

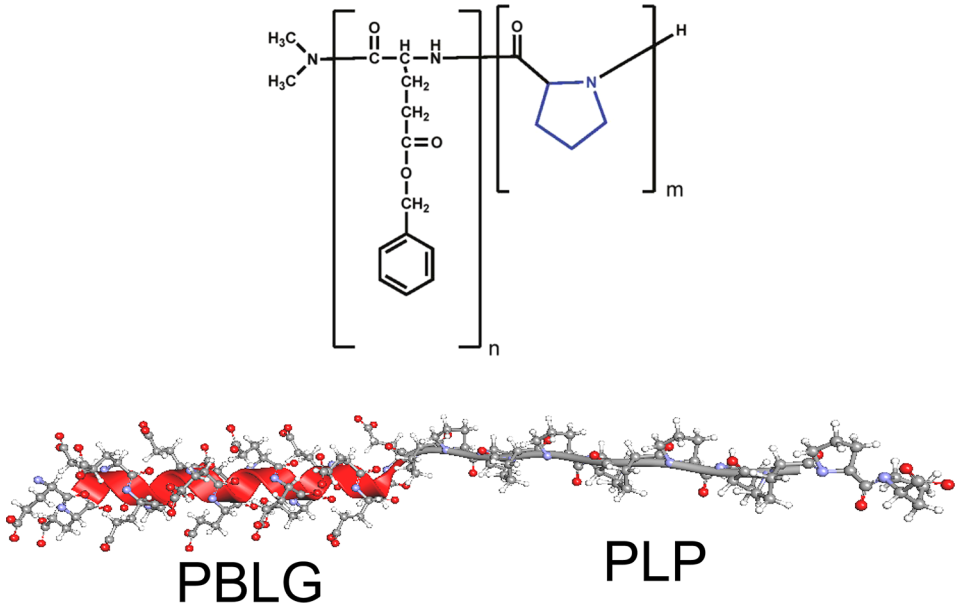


proteins. The localization of these *cis* conformations as well as their role in stabilizing the PBLG and PLP secondary structures in the copolypeptides is explored.

## II. EXPERIMENTAL SECTION

**Synthesis of Poly(L-proline) Homopolypeptides and Poly(γ-benzyl-L-glutamate)-*b*-poly(L-proline) Diblock Copolypeptides.** The synthesis[13] of the poly(L-proline) (PLP) homopolypeptides and the poly(γ-benzyl-L-glutamate)-*b*-poly(L-proline) (PBLG-*b*-PLP) diblock copolypeptides using the high vacuum techniques[14] has been presented in detail elsewhere. Briefly, the synthesis of L-proline *N*-carboxy anhydride (LP-NCA) was performed by reacting *tert*-butyloxycarbonyl-L-proline (Boc-L-proline) with triphosgene in the presence of triethylamine. The formed TEA·HCl salt was removed by filtration and the filtrate was then distilled under vacuum (to remove THF and excess phosgene) and the crude mixture was dried in the high vacuum line. Crude LP-NCA was then dissolved in ethyl acetate, chilled, and extracted with ice-cold water until neutral pH. The organic phase was subsequently separated, filtered, and dried to yield LP-NCA. The purification of crude LP-NCA was carried out by crystallization with a THF/hexane solvent/nonsolvent pair at room temperature. The solid was filtered and was dissolved in warm hexane, and the solution was separated from the solid side products by filtration. Pure LP-NCA crystals were obtained by cooling the LP-NCA solution in hexane at −20 °C and filtration. The purification procedure was repeated until highly purified LP-NCA was obtained. Results are given in Table 1.

**Synthesis of Well-Defined PLP Homopolypeptides.** The synthesis of well-defined poly(L-proline) was performed by dissolving the monomer (LP-NCA) in acetonitrile followed by addition of the initiator dimethylamine. After a few minutes, the solution became turbid and the heterogeneous polymerization was left for one week, with occasional degassing to remove the generated $CO_2$. The final polypeptide (mainly PLP I configuration) was precipitated in cold ether. The purity of the product was verified by SEC-TALLS, FTIR, $^1$H NMR, and $^{13}$C NMR.

**Synthesis of Poly(γ-benzyl-L-glutamate)-*b*-poly(L-proline) (PBLG-*b*-PLP) Copolymers.** γ-Benzyl-L-glutamate-NCA (BLG-NCA) was synthesized according to a previously reported method.[15] The PBLG-*b*-PLP copolymers were synthesized by sequential addition of the BLG-NCA, followed by the addition of LP-NCA after the completion of the polymerization of the first monomer. Briefly, BLG-NCA was dissolved in DMF followed by the addition of the solution of dimethylamine (initiator). The reaction was left for 3 days until completion, with occasional degassing. An aliquot of the solution was removed after the completion of the polymerization for characterization. Then LP-NCA solution in DMF was added. The polymerization was heterogeneous and the final copolypeptide was precipitated in cold ether and dried *in vacuo*. For all polymers, the polypeptides were suspended in Milli-Q water for 3 days under vigorous stirring in order to obtain the water-soluble poly-L-proline II (PLP II) form. Under such conditions PLP form II is expected.

**Table 1. Characteristics of Poly(L-proline) in Homopolymers and in the Copolymers**

| polymer | $M_n$, first block × $10^3$ (g/mol)[a] | *I* of first block | $M_{n,total}$ × $10^3$ (g/mol) | composition of PLP (% w/w)[b] |
|---|---|---|---|---|
| $PBLG_{45}$ | 10.0 | | | |
| $PBLG_{91}$ | 19.9 | 1.06 | | |
| $PLP_{134}$ | 13.0 | 1.24 | | |
| $PBLG_{91}$-*b*-$PLP_{134}$ | 20.0[c] | 1.02 | 33.0[d] | 39[e] |
| $PBLG_{73}$-*b*-$PLP_{300}$ | 16.0[c] | 1.08 | 45.0[d] | 64[e] |

[a]By SEC-TALLS in (0.1 M $NaNO_3$) water/ACN 80:20 at 35 °C. [b]Composition, according to $^1$H NMR in $CF_3COOD$. [c]By SEC in (0.1 M LiBr) DMF at 60 °C. [d]The molecular weights of the PLP block are from stoichiometry, and added to the one of the PBLG obtained by TALLS. [e]Composition according to TGA.

**Solid-State NMR.** The solid state NMR experiments were performed on a Bruker Avance spectrometer with a $^1$H Larmor frequency of 500.1 MHz and $^{13}$C Larmor frequency of 125.76 MHz. A Bruker double resonance probe, supporting rotors of 2.5 mm outer diameter at a spinning frequency of 20 kHz, was used in all cases. At high spinning frequencies, additional heating effects caused by bearing gas friction become significant. The sample temperatures given in this article have been corrected for these frictional heating effects following the procedure of Bielecki et al.[16] For all variable temperature (VT) solid state $^{13}$C cross-polarization (CP) magic angle spinning (MAS) NMR experiments, an initial 90° pulse with 2.5 μs length and 2 s recycle delay were used. The duration of the a variable amplitude


dx.doi.org/10.1021/ma301906m | *Macromolecules* 2012, 45, 9326−9332

contact pulse (80−100%) was 1 ms and the SPINAL64 $^{1}$H decoupling scheme was used while acquiring the $^{13}$C signal. A total of 1k transients were averaged for the experiments. Figure S1 and Figure S2, in the Supporting Information, provide the corresponding $^{13}$C CP-MAS NMR spectra. $^{13}$C{$^{1}$H} heteronuclear correlation spectra with varying spin diffusion delays of 0, 2, and 10 ms have been recorded at a Bruker Avance III spectrometer operating at 850 MHz $^{1}$H Larmor frequency using a commercial double resonance 2.5 mm MAS probe at 25 kHz MAS spinning frequency. Pulse powers, heteronuclear decoupling, and CP-MAS conditions match those of the 1D CP-MAS measurments.

**X-ray Scattering.** Both wide-angle and small-angle X-ray scattering (WAXS/SAXS) measurements have been performed from macroscopically oriented filaments with a diameter of 0.5 mm using a pinhole collimator and a two-dimensional detector (Bruker) with 1024 × 1024 pixels. The extrusion temperatures were 368 and 443 K for **PBLG$_{91}$-*b*-PLP$_{134}$** and **PBLG$_{73}$-*b*-PLP$_{300}$**, respectively. The PLP homopolypeptide was measured in powder form, since it was impossible to extrude. A graphite monochromator was used ($\lambda$ = 0.154 nm), and the sample-to-detector distance was 7.05 cm. Measurements were made within the temperature range from 303 to 453 on heating and on subsequent cooling in steps of 10 K. The recorded 2-D scattered intensities were investigated over the azimuthal angle and are presented as a function of the scattering wave vector $q$ ($q$=($4\pi/\lambda$) sin($2\theta/2$), where $2\theta$ is the scattering angle). Better images were obtained at the highest temperature (453 K) (Figure S3, Supporting Information) suggesting a significant annealing effect. In the SAXS measurements, the sample-to-detector distance was set at 1.78 m and the same extruded fibers were employed as in WAXS. 2-D images were obtained for different temperatures in the range 303 < $T$ < 453 K in 10 K intervals on heating and subsequent cooling.

**Differential Scanning Calorimetry (DSC).** A Mettler Toledo star differential scanning calorimeter was used for the thermal analysis. The copolypeptides were first heated at a rate of 10 K/min to 473 K and subsequently cooled to 133 K with 10 K/min. A second heating run, with the same rate, was used to identify the PBLG glass temperature, $T_g$, as well as other first order transitions. The DSC traces of the homopolypeptides and the two copolypeptides, are displayed in Figure 1. As has been discussed earlier,[17,18,10] the step-like change in the heat flow of **PBLG$_{45}$** associates with the glass temperature originating from mobile amorphous-like segments that connect PBLG $\alpha$-helical segments. In the copolypeptides a similar step is observed over the same temperature range, albeit over a broader temperature range. Apart from the PBLG glass temperature, both copolypeptides display additional features. The **PBLG$_{91}$-*b*-PLP$_{134}$** trace on cooling (not shown here) displays two broad exothermic peaks at 168 and 186 K with respective heats of 2.8 and 9 J/g. On subsequent heating (Figure 1), there are two melting peaks at 229 and 237 K with respective heats of 2.5 and 1.6 J/g. The **PBLG$_{73}$-*b*-PLP$_{300}$** trace on cooling (not shown here) displays two broad and partially overlapping exothermic peaks at 167 and 181 K with a total heat of 14.2 J/g. On subsequent heating (Figure 1) there exist an exothermic peak at 176 K with a heat of 1.8 J/g and two melting peaks at 229 and 237 K with respective heats of 2.9 and 4.3 J/g. These features, which are absent in the homopolypeptide, are likely to reflect some reorganization and liquid crystalline structures at the interface.

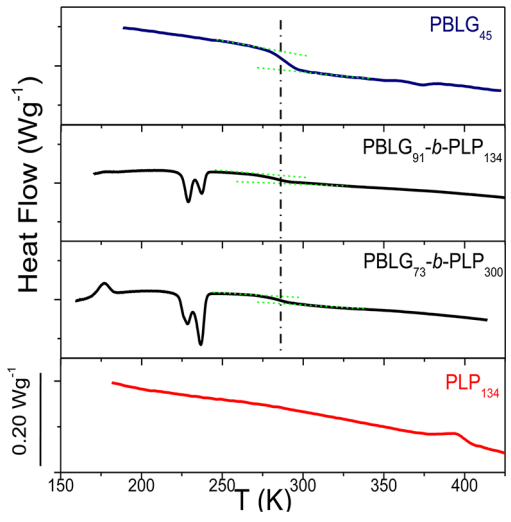


**Figure 1.** DSC thermograms obtained during the second heating run (rate 10 K/min). The glass temperature of PBLG ($T_g^{PBLG}$, shown by the vertical dash-dotted line) remains intact with increasing PLP composition in the diblocks.

## III. RESULTS AND DISCUSSION

**Supramolecular Structure.** The peptide local conformation is conveniently encoded in the $^{13}$C chemical shifts[19] hence the polypeptide secondary structure can be identified using $^{13}$C cross-polarization-magic angle spinning (CP-MAS) solid state NMR. In Figure 2, characteristic $^{13}$C CP-MAS NMR spectra of both homopolypeptides and of the copolymers are shown. PBLG of high molecular weight (DP > 18) is known to form $\alpha$-helices. Indeed, the intense resonances at $\delta \approx$ 176 and 57.5 ppm arise from the amide C═O and $C_\alpha$ carbon, respectively, and indicate the formation of an $\alpha$-helical secondary structure. On the other hand, the **PLP$_{134}$** spectrum exhibits a resonance at $\delta \sim$ 171 ppm corresponding to the PLP ester and resonances at $\delta \sim$ 58.5, 48, 29, and 25 ppm, that correspond to the $C_\alpha$, $C_\delta$, $C_\beta$, and $C_\gamma$, respectively. These resonances are characteristic of helices of PLP. Thus, both homopolypeptides are forming helical structures. The copolypeptides display mixed resonances revealing that both peptides form the same helical secondary structures.

Wide-angle X-ray measurements can provide both the peptide secondary structure and the unit cell in crystalline materials. Representative WAXS images for the homopolypeptides at 423 K are shown in Figure 3. The diffraction pattern of **PBLG$_{45}$** exhibits a set of strong equatorial reflections together with some layer lines. The positions of the lines suggest an $\alpha$-helical conformation of 18 residues in 5 turns (18/5 helix) with a repeat unit of $c$ = 2.7 nm. This structure is described in the literature as the paracrystalline form C; a nematic-like paracrystal with a periodic packing of $\alpha$-helices in the direction lateral to the chain axis. The strong equatorial **PBLG$_{45}$** reflections with ratios 1:3$^{1/2}$:4$^{1/2}$:7$^{1/2}$, indicated with arrows, correspond to the (10), (01), (11), and (20) reflections of a hexagonal unit cell, with lattice parameter $\alpha$ = 1.51 nm, and $d$-spacing given by

$$d_{hex} = \frac{1}{\sqrt{\frac{4}{3a^2}(h^2 + k^2 + hk)}} \quad (1)$$

where $h$ and $k$ are the Miller indices.

The powder **PLP$_{134}$** homopolypeptide employed in the present study exhibits some diffraction peaks at wave vectors 10.82, 12.86, and 17.4 nm$^{-1}$ with corresponding spacings of 0.58, 0.49, and 0.36 nm that correspond well to the (100), (101), and (102) reflections from **PLP$_{134}$** in its form II with a 3$_1$ helical structure. Furthermore, weak reflections at ~18.7 and 21.6 nm$^{-1}$, i.e., at 3$^{1/2}$:4$^{1/2}$ relative to the main peak, suggest also a hexagonal unit cell with a lattice parameter of 0.67 nm.

In the case of the copolypeptides, mixed reflections are present revealing the simultaneous presence of the two hexagonal unit cells. In the copolymer spectra, the PBLG (100) reflections from the hexagonal cell composed of PBLG helices, remain intact independent of block composition


dx.doi.org/10.1021/ma301906m | Macromolecules 2012, 45, 9326−9332

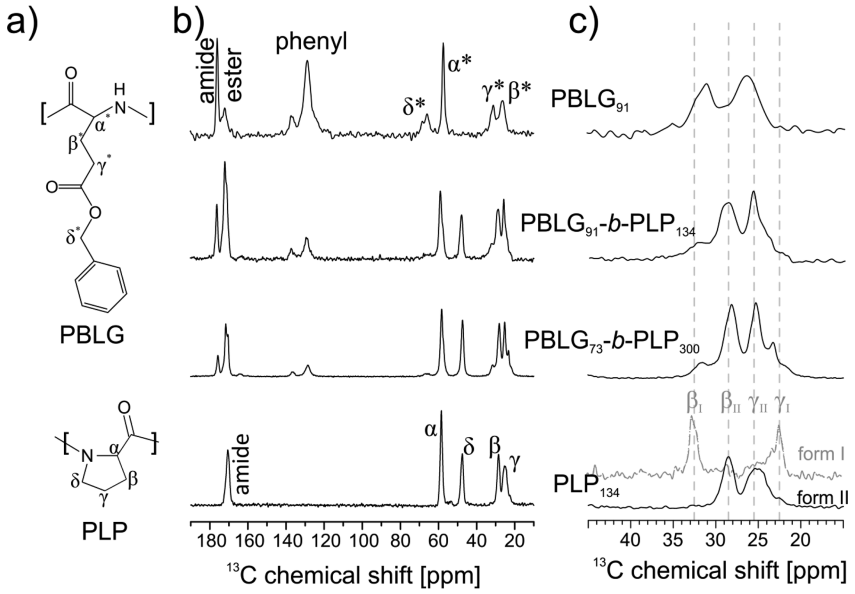


**Figure 2.** $^{13}$C CP MAS NMR spectra for the **PBLG** and **PLP** homopolypeptides and the respective copolypeptides at ambient temperature: (a) Chemical structure of the monomeric units with labels for the assignment of the aliphatic carbon sites; (b) $^{13}$C CP-MAS spectra with the assignment of the different carbon sites, and the chemical shift values of the amide C═O and $C_\alpha$ signals indicate the formation of an $\alpha$-helical secondary structure. The copolymers contain mixed resonances from PBLG and PLP in their helical conformations. (c) Zoom of the $C_\beta$ and $C_\gamma$ signal regions of CP-MAS spectra shown in part b demonstrates that PLP in its II form contains a minority components of form I (positions indicated by dashed gray lines), which increases in the diblock copolymers.

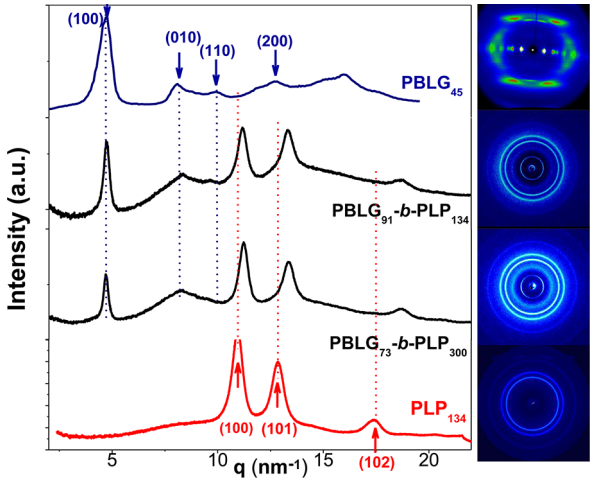


**Figure 3.** Equatorial WAXS intensity distributions of PBLG and PLP homopolypeptides and of the corresponding copolymers obtained from oriented fibers (see text) and measured at 423 K, along with the corresponding 2-D images. The arrows indicate the primary reflections from the hexagonal unit cells of $\mathbf{PBLG_{45}}$ and $\mathbf{PLP_{134}}$. Fiber orientation is along the vertical direction. In the copolymer spectra, the PBLG (100) reflections from the hexagonal cell, remain intact independent from block composition whereas the PLP (100) reflections from the hexagonal unit cell are shifted to higher wavevectors. The 2-D images from the copolypeptides reveal that the PBLG helices are oriented preferably along the fiber axis in contrast to the PLP helices that do not have a preferred orientation.

whereas the PLP (100) reflections from the hexagonal unit cell composed of PLP helices are shifted to higher wavevectors. More importantly, the 2-D images from the copolypeptides reveal that the PBLG helices retain some degree of orientation along the fiber axis (notice the stronger equatorial intensity from the (100) PBLG reflection) in contrast to the PLP helices that remain unoriented. We will return to this point later with respect to the NMR results.

$^{13}$C NMR measurements provide further insight into the PLP conformations. For this purpose the $\mathbf{PLP_{134}}$ polypeptide was measured in both forms (I and II) and the corresponding CP-MAS spectra are shown in Figure 2c at ambient temperature together with the $C_\beta$ and $C_\gamma$ regions of the copolymer CP_MAS spectra and the $\mathbf{PBLG_{91}}$ CP-MAS spectrum. PLP form II at ambient temperature, contains some minor fraction of form I, as shown by the weak $C_{\beta,I}$ and $C_{\gamma,I}$ resonances next to the $C_{\beta,II}$ and $C_{\gamma,II}$ resonances. In the diblocks, a substantial fraction of PLP is found in form I as indicated by the presence of additional resonances at $\delta \sim 32$ ppm corresponding to the $C_\beta$ signal of PLP in form I; this is despite the 3 day stirring the sample in water in order to obtain a complete conversion to PLP form II (see Experimental Section). On heating, the fraction of form I in the diblocks increase further. This is depicted in Figure 4 (with a maximum around 360 K) from the integrated intensities of resonances at $\delta$~28.4 and 32.3 ppm corresponding to the $C_\beta$ signal in form II ($\beta_{II}$) and I ($\beta_I$), respectively. It seems reasonable to attribute these *cis* conformations to the packing frustration at the interface of the PBLG/PLP nanodomains.

In order to probe the spatial proximity of PBLG and PLP moieties and to elucidate further the structure at the interface between PBLG and PLP, two-dimensional $^{13}$C{$^1$H} CP-MAS heteronuclear correlation spectra have been recorded. In the poorly resolved $^1$H MAS spectrum, the signal at 5.5 ppm of the aromatic proton sites at the PBLG phenyl ring are separated from the broad, heavily overlapping proton signals in the aliphatic region of the spectrum. The $^{13}$C{$^1$H} correlation spectrum shown in Figure 5, however, provides sufficient spectral resolution in the better resolved $^{13}$C dimension to unambiguously distinguish different sites of PBLG and PLP. Although the $C_\alpha$, $C_\beta$, and $C_\gamma$ as well as the backbone carbonyl signals of PBLG and PLP overlap, the signals of the PBLG


dx.doi.org/10.1021/ma301906m | *Macromolecules* 2012, 45, 9326−9332

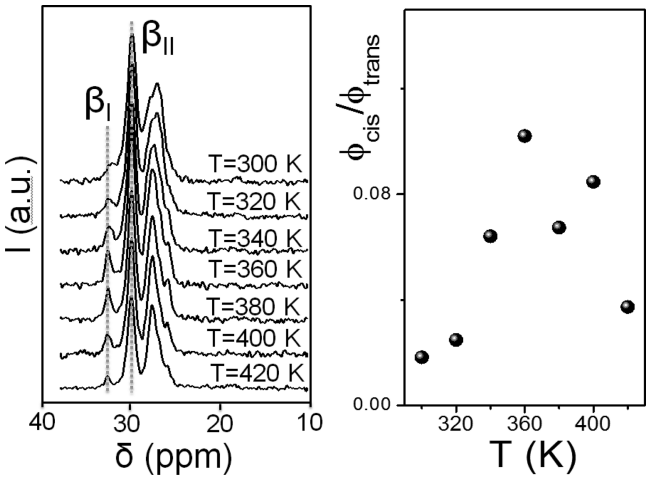


**Figure 4.** (Left) $^{13}$C NMR spectra of **PBLG$_{73}$-*b*-PLP$_{300}$** as a function of temperature. Resonances at $\delta$~28.4 and 32.3 ppm correspond to the $C_\beta$ in form II and I, respectively. (Right) Ratio of the *cis* to *trans* PLP conformations in the diblock obtained from the $C_\beta$ integrated intensities plotted as a function of temperature.

amide group and the aromatic sites as well as the signal from the PLP $C_\delta$ sites are well resolved in the $^{13}$C CP-MAS spectrum. Taking advantage of the spectrally resolved signals of the aromatic PBLG sites in both the $^1$H and the $^{13}$C dimension, two-dimensional spin diffusion experiments were carried out to probe the spatial proximity between PBLG and PLP moieties. The two-dimensional CP-MAS correlation spectrum recorded with a CP contact time of 1 ms shown in Figure 5a indicates correlations between covalently bound $^1$H - $^{13}$C spin pairs or $^1$H and $^{13}$C sites with distances below 0.25 nm. Examples are the aromatic proton (5.5 ppm) and aromatic carbon sites (129 ppm) or the ester carbonyl site of the PBLG side chain (176.4 ppm) and neighboring methylene protons (3.4 ppm).

When a spin diffusion time is introduced into the CP correlation experiment between the proton evolution time and the $^1$H−$^{13}$C CP polarization transfer step, spatial proximities at longer distances can be probed. A spin diffusion time of 2 ms (results shown in Figure 5b) is already sufficient to probe more remote correlations between aromatic proton sites and amide carbonyl sites of the PBLG main chain as well as between aromatic PBLG proton sites and a PLP $C_\delta$ site. Remarkably, there is no contact observed between aromatic protons and the PBLG ester carbonyl site, which should be much closer to the phenyl ring, when elongated PBLG side chains are assumed. This finding indicates that the local mobility of the PBLG side chains has a strong influence on the experimental results and that the spin diffusion occurs primarily through space and not along the chemically bound chains. However, the correlation of the PBLG side chain and the PLP $C_\delta$ site, observed at 2 ms spin diffusion time, demonstrates the presence of a significant interphase between the pure PBLG and PLP phases, where the polypeptides are mixed on the molecular level, and yet preserve their bulk secondary structure. We hurry to point out that at the same spin diffusion time, no contact between the aromatic protons and the ester carbonyl site of the PBLG side chain is observed, emphasizing the close spatial proximity of the aromatic moieties located at the outer surface of the PBLG helix with PLP sites. Since the NMR signals of all other PLP carbon sites overlap with PBLG sites, it is difficult to draw even more detailed conclusions on the local packing. However, for

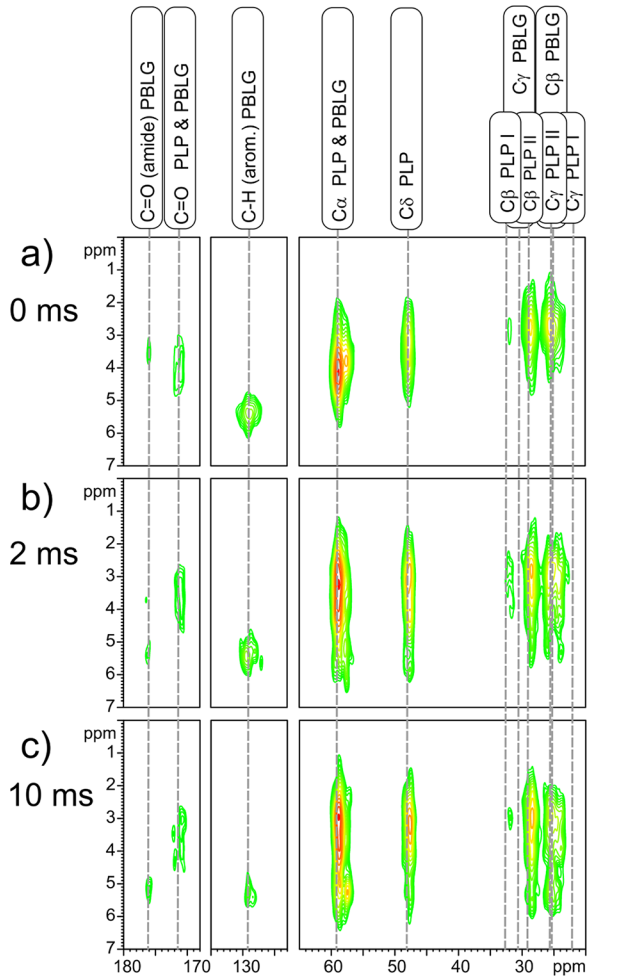


**Figure 5.** Spin diffusion edited $^1$H - $^{13}$C heteronuclear correlation experiments performed at 25 kHz MAS using 1 ms CP contact time for polarization transfer for the **PBLG$_{73}$-*b*-PLP$_{300}$** at ambient temperature. (a) Covalently bound $^1$H − $^{13}$C spin pairs or those with a through space distance below 0.25 nm are probed with the direct CP-MAS correlation experiment (0 ms spin diffusion time). With increasing spin diffusion times $t_m$, (b) $t_m$ = 2 ms and (c) $t_m$ = 10 ms, spatial proximities of $^1$H−$^{13}$C spin pairs with greater internuclear spacings, such as PBLG and PLP contacts, are monitored.

the different $C_\beta$ and $C_\gamma$ sites, where the two different helical structures of PLP can be distinguished. $^1$H−$^{13}$C correlation pattern are observed with minor differences in the $^1$H dimension of the correlation experiments with different spin diffusion times, which can be seen as $^{13}$C detected $^1$H MAS spectra of the proton environment acquired for a specific $^{13}$C site. These differences are difficult to interpret due to the different abundance of the two PLP conformations. The predominant PLP form II is present exclusively within the crystalline regions observed by X-rays, while the relatively strong correlation to the aromatic protons of PBLG detected after 2 ms spin diffusion time at $C_\beta$ of form I indicates the presence of PLP form I in the interphase between crystalline PLP and PBLG. We hurry to point out, that is not the sole PLP conformation at the interface, since a weak correlation of the aromatic proton is observed at $C_\beta$ of form II, where the signals of the interphase in contrast to those of PLP form I are superimposed to the signals of the crystalline PLP regions.

Hence, the NMR results suggest the presence of both helical forms of PLP at the interface being intimately mixed with


dx.doi.org/10.1021/ma301906m | *Macromolecules* 2012, 45, 9326−9332

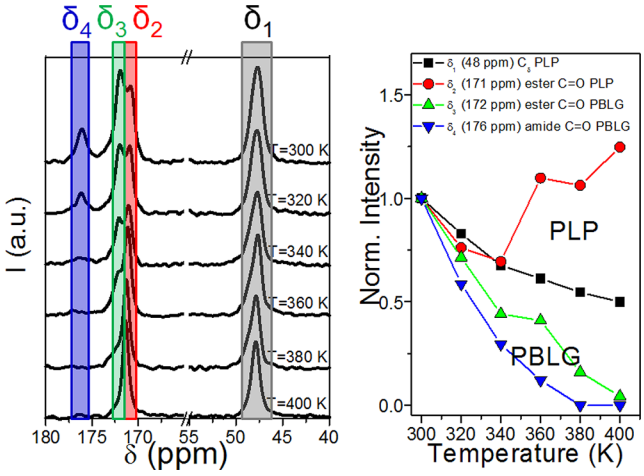


**Figure 6.** (Left) $^{13}C$ NMR spectra of $\mathbf{PBLG_{73}}$-*b*-$\mathbf{PLP_{300}}$ as a function of temperature. Resonances at $\delta_1 \sim 48$ ppm, $\delta_2 \sim 171$ ppm, $\delta_3 \sim 172$ ppm and $\delta_4 \sim 176$ ppm correspond to the PLP $C_\delta$, the PLP ester and to the PBLG side-group ester and amide carbons, respectively. (right) Temperature-dependence of the peak intensities corresponding to the above resonances. Notice the faster intensity drop for the PBLG resonances revealing a mobile PBLG backbone and a relatively rigid PLP backbone at the MAS spinning frequency ($\omega = 2\pi f$, $f = 20$ kHz).

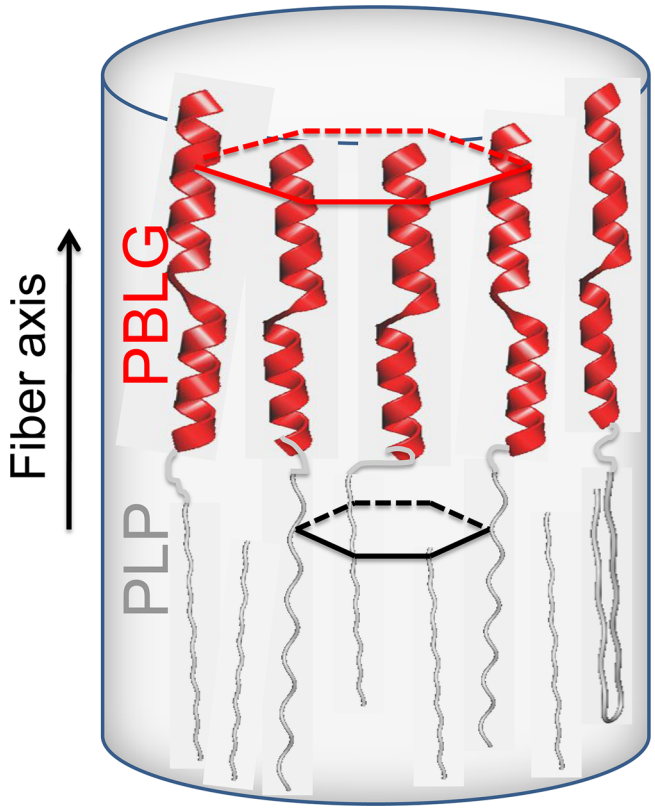


**Figure 7.** Highly schematic representation of the copolymer self-assembly showing PBLG and PLP $\alpha$-helices (NMR, WAXS) that are hexagonally packed (WAXS). The respective unit cells are indicated with red and black lines.

PBLG moieties. The *cis* PLP conformations at the crystalline PLP/PBLG interface alleviate the packing frustration and permit for PBLG and PLP helices to pack preserving their bulk properties. The presence of *cis* conformations in the interphase between crystalline PLP and PBLG regions can also explain the absence of a specific orientation of PLP chains in the X-ray images of the extruded fibers. These structural findings are schematically depicted below with respect to Figure 7. The figure displays hexagonally packed PBLG and PLP $\alpha$-helices possessing very different unit cells and an interface that is rich in PLP *cis* conformations. Under these restrictions, PLP chains obtain their bulk density by interdigitation.

**Rigidity of Peptide Secondary Structures.** The DSC results revealed the presence of a PBLG glass temperature in the copolymers without an indication for a second (PLP) glass temperature. This suggested very different mobilities for the two polypeptides. Information on the rigidity/dynamics of both polypeptides can also be obtained from $^{13}C$ NMR spectra recorded as a function of temperature.[20] NMR profiles (Figure 2b) showed two nonoverlapping resonances at $\delta_1 \sim 48$ and $\delta_4 \sim 176$ ppm corresponding to the $C_\delta$ PLP and PBLG amide C=O, respectively. In addition, the partially overlapping resonances at $\delta_2 \sim 171$ ppm and $\delta_3 \sim 172$ ppm correspond to the amide PLP and side-group ester of PBLG, respectively. All of the above can be employed as fingerprints of the PBLG and PLP dynamics by recording temperature-dependent spectra. Such spectra are depicted in Figure 6 for the $\mathbf{PBLG_{73}}$-*b*-$\mathbf{PLP_{300}}$ over the interesting spectral regions. Evidently, the PLP $C_\delta$ and PBLG amide C=O resonances show distinctly different *T*-dependences. The former resonance loses about 40% of its integrated intensity in the *T*-range from 300 to 400 K, whereas the latter reduces to a level that cannot be distinguished from the background noise. These intensity losses occur because the local peptide dynamics interfere with the magic angle spinning, cross-polarization, and dipolar decoupling all of the order of 20 kHz.[21,22] Hence, the intensity corresponding to the $\delta_3 \sim 172$ ppm and $\delta_4 \sim 176$ ppm resonances of PBLG is minimized at ~400 K suggesting that the underlying motional rates are about 20 kHz. As discussed earlier, this intensity drop for PBLG signifies low amplitude backbone motions of $\alpha$-helical segments. However, within the same *T*-range, the PLP dynamics is less affected. The results show a mobile PBLG backbone and a relatively rigid PLP backbone at the NMR frequency over the investigated *T*-range. This is consistent with the pronounced phase separation of the two polypeptides, where PBLG has a lower glass temperature and further indicates a much higher glass temperature for PLP. The relative rigidity of PLP is also consistent with its use as a spectroscopic reference in single-molecule fluorescence experiments (i.e., spectroscopic ruler).[23,24]

## IV. CONCLUSION

Copolypeptides of PBLG and PLP form $\alpha$-helical secondary structures corresponding to both PBLG and PLP segments stabilized, respectively, via hydrogen bonding and steric hindrance. In both domains the helices were hexagonally packed possessing however very different lattice constants of 1.51 nm for PBLG and 0.67 nm for PLP. In fibers, the PBLG helices are preferentially oriented along the fiber axis, whereas the PLP helices were found to be unoriented. Combined NMR and X-ray studies revealed that the dissimilar lateral packing constraints of the two peptides at the interface give rise to a packing frustration that is relieved by a *trans*/*cis* conformational transition of the PLP block. The resulting *trans*/*cis* change of the PLP conformations allows intedigitation of the PLP helices and mimics the isomerization of isolated proline residues in proteins. The interfacial organization of PLP in model


dx.doi.org/10.1021/ma301906m | *Macromolecules* 2012, 45, 9326−9332

copolypeptides may thus provide more insight into the role of proline residues as helical "brakers" or helical redirectors.

## ■ ASSOCIATED CONTENT

### Ⓢ Supporting Information

$^{13}$C CP MAS spectra and wide-angle X-ray scattering spectra. This material is available free of charge via the Internet at http://pubs.acs.org.

## ■ AUTHOR INFORMATION

### Notes

The authors declare no competing financial interest.

## ■ ACKNOWLEDGMENTS

This work was cofinanced by the E.U.—European Social Fund and the Greek Ministry of Development—GSRT in the framework of the program THALIS. Financial support of the Deutsche Forschungsgemeinschaft, SFB 625 is gratefully acknowledged. H.I and M.G. acknowledge the financial support of the Hellenic Ministry of Education through Herakleitos II program, cofinanced from the operational program EPEAK and the European Social Funds.

## ■ REFERENCES

(1) Cowan, P. M.; McGavin, S.; North, A. C. T. *Nature* **1955**, *176*, 1062−1064.
(2) Cowan, P. M.; McGavin, S. *Nature* **1955**, *176*, 501−503.
(3) Brandl, C. J.; Deber, C. M. *Proc. Natl. Acad. Sci. U.S.A.* **1986**, *83*, 917−921.
(4) MacArthur, M. W.; Thornton, J. M. *J. Mol. Biol.* **1991**, *218*, 397−412.
(5) Barlow, D. J.; Thornton, J. M. *J. Mol. Biol.* **1988**, *201*, 601−619.
(6) Schimmel, P. R.; Flory, P. J. *Chemistry* **1967**, *58*, 52−59.
(7) Walton, A,G.; Blackwell, J. *Biophysics*; Academic Press: New York, 1973.
(8) Deber, C. M.; Bovey, F. A.; Carver, J. D.; Blout, E. R. *J. Am. Chem. Soc.* **1970**, *92*, 6191−6198.
(9) Floudas, G.; Papadopoulos, P.; Klok, H.-A.; Vandermeulen, G. W. M.; Rodriguez-Hernandez, J. *Macromolecules* **2003**, *36*, 3673−3683.
(10) Papadopoulos, P.; Floudas, G.; Klok, H.-A.; Schnell, I.; Pakula, T. *Biomacromolecules* **2004**, *7*, 81−91.
(11) Klok, H.-A.; Lecommandoux, S. *Adv. Polym. Sci.* **2006**, *202*, 75.
(12) Floudas, G.; Spiess, H. W. *Macromol. Rapid Commun.* **2009**, *30*, 278−298.
(13) Gkikas, M.; Iatrou, H.; Thomaidis, N. S.; Alexandridis, P.; Hadjichristidis, N. *Biomacromolecules* **2011**, *12*, 2396−2406.
(14) Hadjichristidis, N.; Iatrou, H.; Pispas, S.; Pitsikalis, M. *J. Polym. Sci.* **2000**, *38* (Part A), 3211−3234.
(15) Aliferis, T.; Iatrou, H.; Hadjichristidis, N. *Biomacromolecules* **2004**, *5*, 1653−1656.
(16) Bielecki, A.; Burum, D. *J. Magn. Reson. A* **1995**, *116*, 215−220.
(17) Papadopoulos, P.; Floudas, G.; Schnell, I.; Klok, H.-A.; Aliferis, T.; Iatrou, H.; Hadjichristidis, N. *J. Chem. Phys.* **2005**, *122*, 224906.
(18) Gitsas, A.; Floudas, G.; Mondeshki, M.; Lieberwirth, I.; Spiess, H. W.; Iatrou, H.; Hadjichristidis, N.; Hirao, A. *Macromolecules* **2010**, *43*, 1874.
(19) Tonelli, A. E. *NMR Spectroscopy and Polymer Microstructure*, Wiley-VCH: Weinheim, Germany, 1989.
(20) Gitsas, A.; Floudas, G.; Mondeshki, M.; Spiess, H. W.; Iatrou, H.; Hadjichristidis, N. *Macromolecules* **2008**, *41*, 8072.
(21) Maricq, M. M.; Wauch, J. J. *J. Chem. Phys.* **1979**, *70*, 3300.
(22) Suwelack, D.; Rothwell, W. P.; Wauch, J. S. *J. Chem. Phys.* **1980**, *73*, 2559.
(23) Schuler, B.; Lipman, E. A.; Steinbach, P. J.; Kumke, M.; Eaton, W. A. *Proc. Natl. Acad. Sci. U.S.A.* **2005**, *102*, 2754.
(24) Schuler, B.; Lipman, E. A.; Eaton, W. A. *Nature* **2002**, *419*, 743.